Voltage Unbalance Compensation in Distribution Feeders Using Soft Open Points

Rui You and Xiaonan Lu

***Abstract*—Soft open points (SOPs) are power electronic devices that may replace conventional normally-open points in distribution networks. They can be used for active power flow control, reactive power compensation, fault isolation, and service restoration through network reconfiguration with enhanced operation flexibility and grid resiliency. Due to unbalanced loading conditions, the voltage unbalance issue, as a common problem in distribution networks, has negative impacts on distribution network operation. In this paper, a control strategy of voltage unbalance compensation for feeders using SOPs is proposed. With the power flow control, three-phase current is regulated simultaneously to mitigate the unbalanced voltage between neighboring feeders where SOPs are installed. Feeder voltage unbalance and current unbalance among three phases are compensated with the injection of negative-sequence and zero-sequence current from SOPs. Especially in response to power outages, three-phase voltage of isolated loads is regulated to be balanced by the control of SOPs connected to the feeders under faults, even if the loads are unbalanced. A MATLAB/Simulink model of the IEEE 13-bus test feeder with an SOP across feeder ends is implemented, and experimental tests on a hardware-in-the-loop platform are implemented to validate the effectiveness of the proposed control strategy.**

***Index Terms*—Distribution network, service restoration, soft open point (SOP), voltage unbalance compensation.**

I. Introduction

In recent years, distributed generators (DGs) such as wind turbines and photovoltaics have been integrated into distribution networks due to the economic and environmental concerns of conventional energy resources [1], [2]. The intermittency and variability of high-penetration DGs make the operation and control of distribution networks relatively more complex and challenging [3]. This is because traditional distribution networks usually exhibit radial structures considering the need of reliable isolation of network faults with simple protection strategies. They are designed to be passive feeders supplying the load demands from the generation side [4]. Therefore, power flow is supposed to be unidirectional. However, considering the integration of distributed energy resources, there could be reverse power flow in conventional distribution feeders that may jeopardize the operation of existing grid equipment, e.g., protective devices, etc., and impose other operational issues, e.g., voltage violation, excessive current or voltage harmonics, etc. [5].

Among the preceding issues mentioned above, voltage unbalance is also very common in distribution feeders, and may have significant impacts on distribution network operation. Asymmetric three-phase line configuration and numerous single-phase loads lead to unbalanced distribution networks. The unbalanced condition is further deteriorated due to asymmetric integration of DGs [6], which results in the voltage unbalance in different sections of distribution networks. Under unbalanced conditions, the distribution network undergoes more losses and potential instabilities. Moreover, the voltage unbalance has adverse effects on the equipment such as power electronic devices and adjustable speed drives [7]. Therefore, it is desirable to establish the controllable link between unbalanced sections to mitigate the unbalanced condition collaboratively.

Conventional voltage regulation approaches are mainly on primary equipment such as on-load tap changers, switchable capacitor banks, and tie switches [8]. Due to the slow response and discrete voltage regulation, it is hard to meet the requirement of rapid voltage regulation [9]. In order to solve the fast voltage variation due to the cloud movement over the photovoltaic systems, the use of static var compensators, distribution-level static synchronous compensator (STATCOM) [10], and voltage sourced converter (VSC) based DG [11] has been proposed in the literature. However, these conventional approaches only focus on single point of interconnection for unbalance compensation. It is noteworthy that the controllability and flexibility of network operation can be enhanced with flexible interconnection with soft open points (SOPs) [12], [13]. The benefits of SOPs in both radial and looped (mesh) networks can be obtained, and the drawbacks can be avoided [14]. SOPs refer to power electronic devices that can be used to replace conventional normally-open points (NOPs), which locate at the end of distribution feeders to interconnect neighboring feeder ends, as shown in Fig. 1 [15]-[18]. Rather than simply switching on and off, SOPs can provide versatile functionalities compared with leg-

Manuscript received: August 16, 2021; revised: December 19, 2021; accepted: March 15, 2022. Date of CrossCheck: March 15, 2022. Date of online publication: May 26, 2022.

The work of R. You was supported by Shandong Provincial Key Research and Development Program (No. 2019JZZY010902) and Shandong Provincial Natural Science Foundation (No. ZR2020ME197).

R. You (corresponding author) is with the College of Electrical Engineering, Qingdao University, Qingdao 266071, China (e-mail: yourui1984@163.com).

X. Lu is with the College of Engineering, Temple University, PA 19122, USA (e-mail: xiaonan.lu@ieee.org).

DOI: 10.35833/MPCE.2021.000565

acy NOPs, including balancing feeder loading, regulating feeder end voltage, service restoration after faults, etc. [19], [20]. Their engineering applications can be found in [21]. SOPs continuously regulate active power and reactive power of the connected feeders, resulting in the collaborative control on voltage unbalance [22], [23].

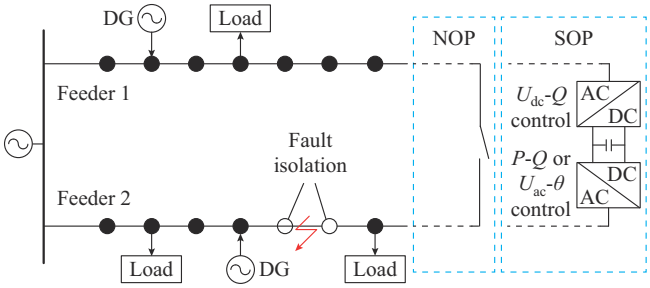

Fig. 1. Schematic of installation and operation of SOP in distribution network.

In terms of three-phase voltage unbalance compensation with SOPs, there is limited work done in this area. An optimal operation strategy is proposed to mitigate the three-phase voltage unbalance while minimizing power losses simultaneously in [24]. A stochastic scenario-based optimal sizing and siting model of SOPs for mitigating three-phase voltage unbalance in distribution networks considering DG and load uncertainties is proposed in [25]. However, the focus is on the power flow optimization in the distribution networks. The control strategy of voltage and current unbalance compensation among three phases during normal network operation and under critical load restoration conditions has not been explored.

To fill the gap, a control strategy of comprehensive voltage unbalance compensation on feeders using SOPs is proposed in this paper. Compared with the existing voltage unbalance compensation methods for distribution feeders, the main contributions of this paper are as follows.

1) Voltage unbalance among three phases at the interconnected feeders is compensated with the injection of negative-sequence and zero-sequence currents from SOPs.

2) Three-phase current is regulated simultaneously at the same time to improve the voltage unbalance between neighboring feeders where SOPs are installed with flexible power flow control.

3) Balanced three-phase voltage is generated to support isolated loads for service restoration, even if the loads are unbalanced.

4) The compensation control above can be achieved independently on all feeders where SOPs are installed.

The rest of this paper is organized as follows. Section II presents the operation principle of SOPs in distribution networks. A control strategy is designed in Section III. A model including the IEEE 13-bus test feeder with an SOP and case studies are given in Section IV. Experiments on a hardware-in-the-loop platform are implemented to illustrate the effectiveness of the proposed control strategy in Section V. Finally, the conclusions are drawn in Section VI.

II. Operation Principle of SOPs in Distribution Networks

A two-feeder distribution network is interconnected with a back-to-back VSC based SOP, in replacement of a conventional NOP, as shown in Fig. 1. Compared with the NOP, the SOP can control power flow precisely with lower operation costs. The risk caused by frequent switching actions is avoided. Therefore, the operational flexibility and resiliency of distribution networks can be improved significantly [26].

Under normal network operation conditions, the power flow can be controlled for the improvement of feeder load balance and power loss reduction. In addition, network voltage can also be regulated for increased DG penetration levels, which can be further elevated using SOPs with energy storage devices [27], [28]. Independent reactive power can be supplied or absorbed at both terminals of the SOP. One converter operates in the P-Q control mode to control its active power P and reactive power Q, while the other one operates in the U_{dc}-Q control mode to stabilize DC-link voltage U_{dc} and regulate reactive power.

Under fault operation condition, if a fault occurs on one feeder, the fault is isolated from the other one due to the SOP overcurrent limit. After the fault is isolated, the connected converter will be switched to the U_{ac}-θ control mode to re-allocate load demands and support critical load restoration with the amplitude U_{ac} and phase angle θ efficiently. Furthermore, the other converter will operate in the U_{dc}-Q control mode. Therefore, the voltage support and service restoration in the unfaulted areas are also achieved [29].

Under the above two conditions, two kinds of voltage unbalance issues exist. To realize the functions above and solve the voltage unbalance issues, a control strategy with two modes is proposed. The detailed analysis of the above issues and the corresponding control strategy will be discussed in the next section.

III. Control Strategy of SOPs for Voltage Unbalance Mitigation

The circuit topology of a back-to-back VSC based SOP is shown in Fig. 2. It is similar to two STATCOMs with a common DC bus. However, the original main functions (power flow optimization and service restoration) of SOPs all involve active power control, while STATCOMs are used for the reactive power compensation, unbalance compensation, and harmonic control. Since the voltage unbalance compensation can be achieved with a VSC in a STATCOM, SOPs are also expected to have the capability and contribute to the unbalance improvement.

Under normal network operation conditions, if three-phase loads, e. g., load 1 and load 2, are unbalanced, unbalanced three-phase load current will occur, which deteriorates the three-phase unbalanced voltage of the feeder. When the SOP operates in the service restoration, the balanced three-phase voltage generated from the connected converter will result in unbalanced three-phase load voltage. This is because the three-phase inductance L used to attenuate high-frequency harmonics is the same. Unbalanced three-phase load current leads to the unbalanced three-phase load voltage.

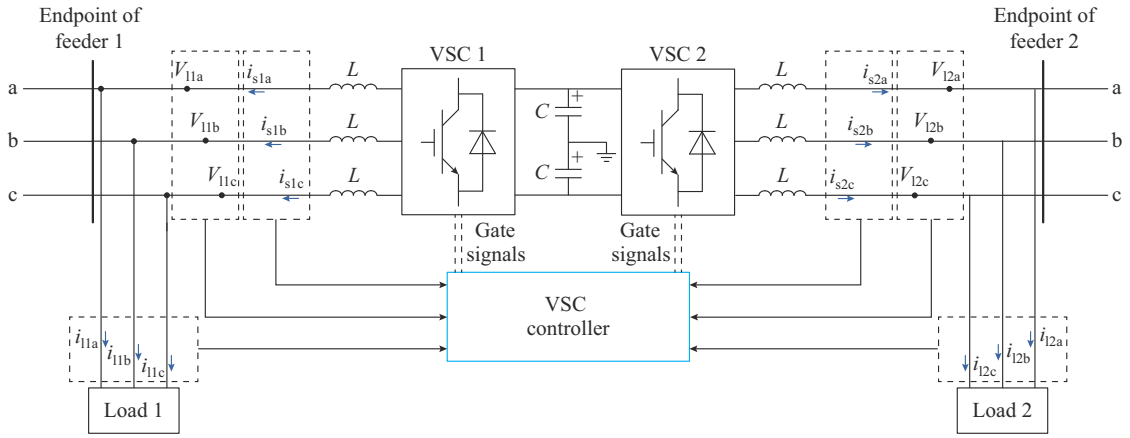

Fig. 2. Circuit topology of a back-to-back VSC based SOP.

In order to compensate the unbalanced voltage, a control strategy with two control modes is proposed. Under normal network operation and service restoration, three-phase current unbalance compensation control and three-phase load voltage balance control are applied, respectively, which will be detailed below.

A. Three-phase Current Unbalance Compensation Control

Taking load 1 in Fig. 2 as an example, the unbalanced load leads to the unbalanced three-phase currents i_{l1a}, i_{l1b}, and i_{l1c}, which are the sum of the positive-, negative-, and zero-sequence components in (1).

$$\begin{bmatrix} i_{l1a} \\ i_{l1b} \\ i_{l1c} \end{bmatrix} = i_{l1p}\begin{bmatrix} \cos(\omega t+\varphi_p) \\ \cos(\omega t-120°+\varphi_p) \\ \cos(\omega t+120°+\varphi_p) \end{bmatrix} + i_{l1n}\begin{bmatrix} \cos(\omega t+\varphi_n) \\ \cos(\omega t+120°+\varphi_n) \\ \cos(\omega t-120°+\varphi_n) \end{bmatrix} + i_{l10}\begin{bmatrix} \cos(\omega t+\varphi_0) \\ \cos(\omega t+\varphi_0) \\ \cos(\omega t+\varphi_0) \end{bmatrix} \tag{1}$$

where i_{l1p}, i_{l1n}, and i_{l10} are the amplitudes of the positive-, negative-, and zero-sequence load currents, respectively; φ_p, φ_n, and φ_0 are the phase angles of positive-, negative-, and zero-sequence currents, respectively; and ω is the angular frequency. If the negative- and zero-sequence currents are generated by VSC 1, only the positive-sequence current is supported from feeder 1. This means that the feeder current is controlled to be balanced, contributing to the three-phase voltage unbalance mitigation of the feeder. The diagram with three-phase current unbalance compensation control is shown in Fig. 3.

The power flow control is presented firstly. One of the two VSCs controls the active power to one feeder P according to its reference P^*, and the other one stabilizes the DC-link voltage V_{dc} according to its reference V_{dc}^*. The active power loop or the DC-link voltage loop is used to generate the current reference, i.e., the d-axis current component i_d^*. The reactive power to the connected feeder is controlled individually by the two VSCs. Meanwhile, the reactive power error is transformed into the q-axis current component i_q^*. Two limiters are used to achieve current limiting in i_d^* and i_q^* during system faults and disturbances. Three-phase reference currents of VSC, i_a^*, i_b^*, and i_c^*, are calculated based on the voltage phase angle of the feeder. The angle is calculated from a phase locked loop (PLL), whose input is the positive-sequence voltage component extracted from the instantaneous feeder voltages V_{la}, V_{lb}, and V_{lc} based on the nominal angular frequency ω^* [30]. The reference currents of VSC, i_{sa}^*, i_{sb}^*, and i_{sc}^*, are compared with the measured output currents i_{sa}, i_{sb}, and i_{sc} to determine gate signals of insulated gate bipolar transistor (IGBT). The load current unbalance compensation between the two feeders connected by the SOP is realized.

Negative-sequence current injection control and zero-sequence current injection control are illustrated below. The measured three-phase load currents i_{la}, i_{lb}, and i_{lc} are transformed into the d- and q-axis components i_{ld}^* and i_{lq}^* based on $-\theta$. Further, the DC components, corresponding to the negative-sequence current components, are extracted through moving average filters (MAFs). The MAF is performed as a low pass filter [31] as shown in (2).

$$\bar{x}(t) = \frac{1}{T_w}\int_{t-T_w}^{t} x(\tau)\mathrm{d}\tau \tag{2}$$

where T_w is the window width, whose corresponding frequency is the frequency of input signal sinusoidal components; and $\bar{x}(t)$ is the average value of the input signal. The d- and q-axis current components determined from proportional integral (PI) controllers are transformed into three-phase negative-sequence current references Δi_{na}^*, Δi_{nb}^*, and Δi_{nc}^* based on $-\theta$. The feeder current unbalance among three phases is compensated by adding these references to the power flow reference current. If the three-phase four-wire network is used, the zero-sequence load current may also exist. Therefore, the zero-sequence current also needs to be generated from the VSCs. The calculated zero-sequence current component Δi_{nz}^* is also added to achieve the current unbalance compensation. In this case, the generation route of zero-sequence current must be provided in terms of the circuit topology such as the split-capacitor in Fig. 2. The feeder current unbalance among the three phases can be independently compensated by the two VSCs, due to the decoupling function of DC-link capacitor in the SOP.

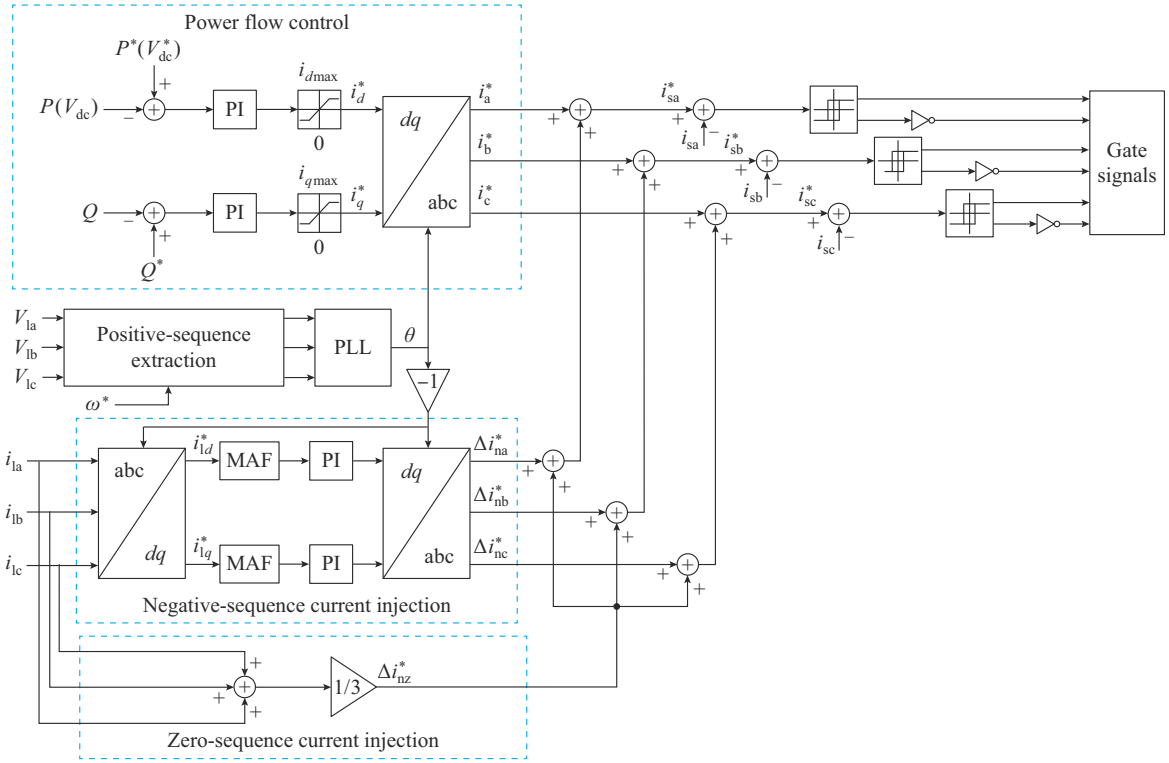

Fig. 3. Diagram with three-phase current unbalance compensation control.

This means that three-phase current unbalance compensations for feeder 1 and feeder 2 are achieved by VSC 1 and VSC 2, respectively. Furthermore, the current unbalance compensation control on more connected feeders can be achieved individually by more VSCs for multi-terminal SOPs.

B. Three-phase Load Voltage Balance Control

When load 1 is isolated due to fault occurrence on feeder 1, VSC 1 should operate in the U_{ac}-θ control mode to realize the service restoration. Balanced three-phase voltage is generated at load 1 with the control diagram presented in Fig. 4, where PWM stands for paulse width modulation and PR stands for proportional resonance.

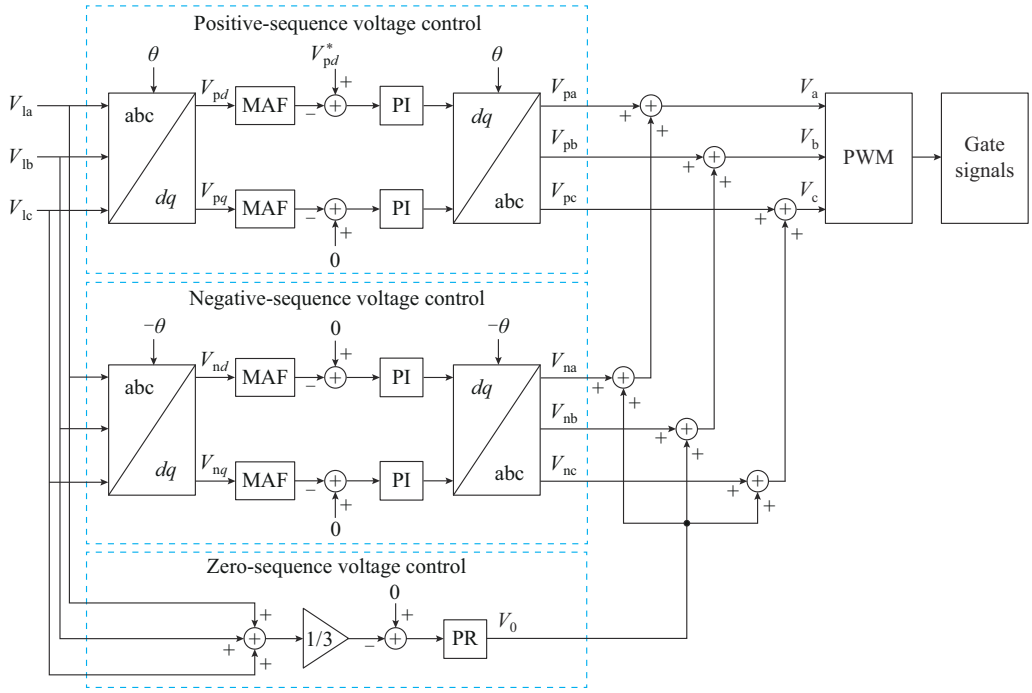

Fig. 4. Block diagram of three-phase load voltage balance control.

The measured three-phase voltage of load 1 is transformed into the d- and q-axis components V_{pd} and V_{pq}. Different from the three-phase current unbalance compensation control, θ is generated inherently with the integral of the nominal frequency. Both AC and DC components exist in the dq-axis components. MAFs are used to extract the DC components, corresponding to positive-sequence voltage components [32]. The d-axis reference voltage V_{pd}^{*} is calculated as:

$$V_{pd}^{*} = \sqrt{2/3}\, V_{rms} \tag{3}$$

where V_{rms} is the nominal line to line root mean square voltage of load 1. The q-axis reference voltage V_{pq}^{*} is set to be 0. Errors are used to calculate the output voltage components of VSC 1 in the d- and q-axis. At last, they are transformed into the three-phase positive-sequence voltages V_{pa}, V_{pb}, and V_{pc}.

In order to eliminate the negative-sequence voltage at load 1, negative-sequence reference voltage components in the d- and q-axis are both set to be 0. Similar to the positive-sequence voltage control, three-phase negative-sequence compensation voltage V_{na}, V_{nb}, and V_{nc} can be calculated according to the dq-axis components V_{nd} and V_{nq}. The only difference is that $-\theta$ is used for the coordinate transformation. If load 1 is supplied from the three-phase four-wire network originally, zero-sequence voltage compensation control should also be applied. Zero-sequence compensation voltage V_0 is calculated with a PR controller, whose input signal is the error between actual zero-sequence voltage and reference zero-sequence voltage at load 1. The calculated negative-sequence voltage and zero-sequence compensation voltage are added to the positive-sequence voltage to obtain the final three-phase voltages V_a, V_b, and V_c and achieve the voltage balance control at load 1.

VSC 2 operates in the U_{dc}-Q control mode to stabilize the DC-link voltage. Furthermore, the three-phase current unbalance compensation control of the feeder mentioned above can still be used to mitigate the current unbalance at feeder 2. The delay between the fault occurrence and service restoration exists. This is due to the requirements for isolating a permanent fault and guaranteeing the generation restoration for distribution automation [26]. Therefore, there is enough time to finish the control mode transition of load 1 from U_{dc}-Q or P-Q control mode to U_{ac}-θ control mode.

IV. Simulation Results

The IEEE 13-bus test feeder model is built in MATLAB/Simulink to verify the effectiveness of the control strategy for voltage unbalance compensation under different network operation conditions. An SOP is connected between node 633 and node 692 in Fig. 5.

System parameters are shown in Table I. An average model of the SOP is used, and losses, harmonics, and fast switching transients of its two VSCs are neglected. The three-phase current unbalance compensation control and three-phase load voltage balance control are studied, respectively. The two cases and simulation results are presented below.

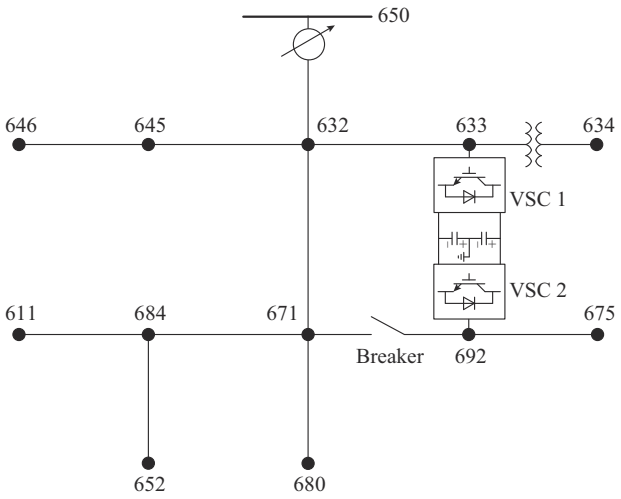

Fig. 5. Configuration of IEEE 13-bus test feeder model with an SOP.

TABLE I
System Parameters

Parameter	Value
DC-link capacitor	1000 μF
DC-link rated voltage	7.2 kV
Filter inductor	2 mH
Rated line-to-line voltage of VSC	4.16 kV
Rated power of SOP	1 MVA

A. Three-phase Current Unbalance Compensation Control Under Normal Network Operation Condition

VSC 1 is controlled to stabilize the DC-link voltage. The negative-sequence current is injected gradually from 0.1 s, and is kept stable after 0.2 s. The zero-sequence current injected increases gradually from 0.2 to 0.3 s.

The negative-sequence current and zero-sequence current injected from VSC 2 increase gradually from 0.3 to 0.4 s and from 0.4 to 0.5 s, respectively. The power flow control is enabled from 0.5 s to balance the loading of node 633 and node 692. The output power of VSC 2 increases gradually from 0.5 s and is kept stable after 0.6 s.

The output current of VSC 1 i_{VSC1} composed of its positive-sequence component i_p, negative-sequence component i_n, and zero-sequence component i_z is show in Fig. 6.

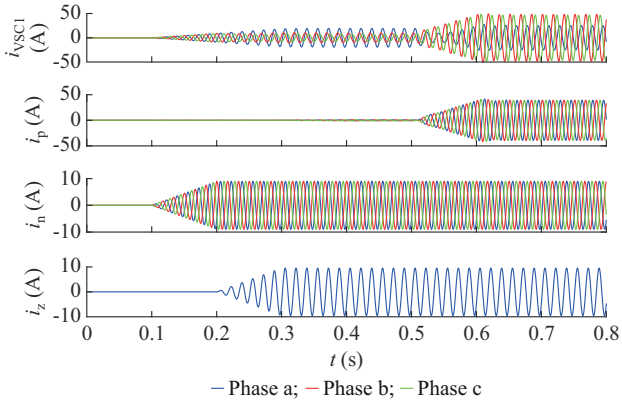

Fig. 6. Output current of VSC 1 composed of i_p, i_n, and i_z.

Since three-phase zero-sequence current injected is identical, only zero-sequence current of phase a is displayed. The output current of VSC 2 i_{VSC2} including each sequence component is shown in Fig. 7. The currents of node 633 and node 692 are shown in Fig. 8 and Fig. 9, respectively. The currents from 0 to 0.1 s, and from 0.7 to 0.8 s are shown in Fig. 10 and Fig. 11, respectively. It can be observed that the unbalanced loads lead to unbalanced currents of node 633 and node 692 in terms of both the amplitude and the phase. With the injection of negative-sequence current and zero-sequence current, the node current is controlled to be balanced successfully.

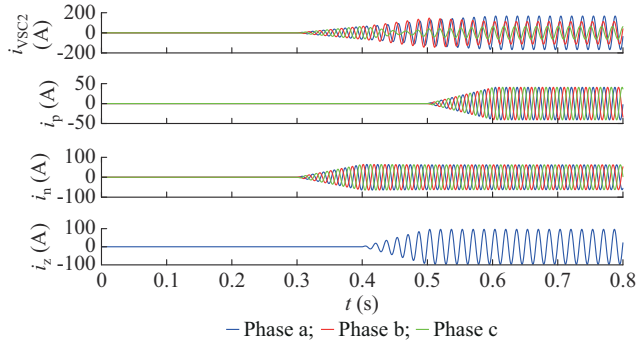

Fig. 7. Output current of VSC 2.

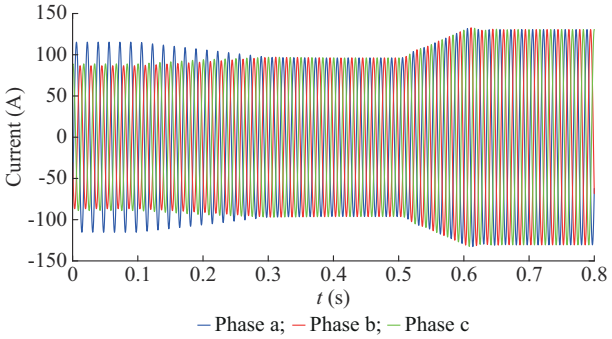

Fig. 8. Current of node 633.

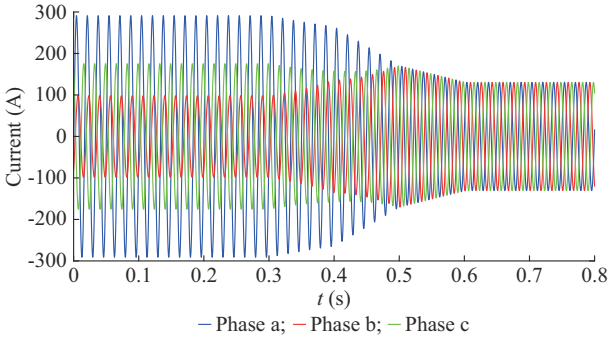

Fig. 9. Current of node 692.

The DC-link voltage is shown in Fig. 12. The current injection introduces the DC-link voltage oscillation with 120 Hz of doubled network frequency. However, the average voltage is almost constant, and the stable DC-link voltage is kept. From $t = 0.5$ s, the increase of positive-sequence current of VSC 2 results in the dropping of DC-link voltage.

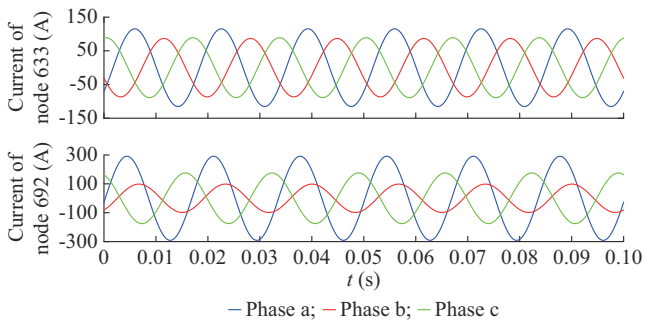

Fig. 10. Currents of node 633 and node 692 from 0 to 0.1 s.

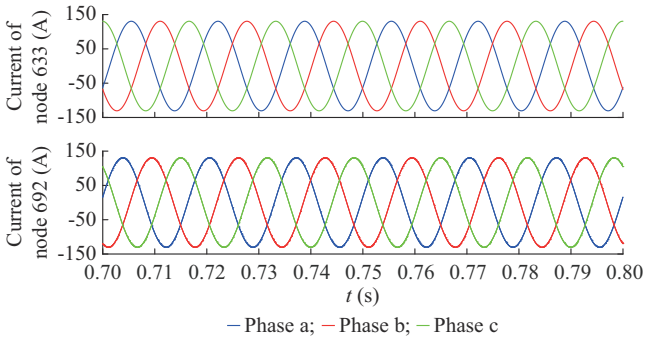

Fig. 11. Currents of node 633 and node 692 from 0.7 to 0.8 s.

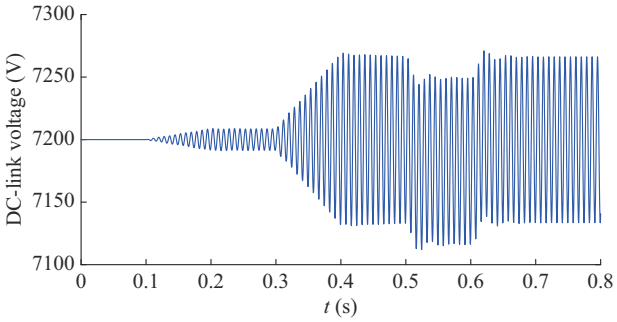

Fig. 12. DC-link voltage.

With the positive-sequence current adjustment from VSC 1, the DC-link voltage is stabilized successfully. With the power flow control, the same amplitude of the three-phase balanced node current (about 130 A) is obtained finally.

It should be noted that if two STATCOMs, also employing two VSCs, are installed at node 633 and node 692, the node current unbalance compensation among three phases can also be obtained. However, the power flow with the positive-sequence current control cannot be achieved. The SOP advantages over that of two STATCOMs are verified.

Voltages of node 633 and node 692 are shown in Fig. 13. Though the improvement on the node current unbalance is obvious, it is not true for the improvement of node voltage unbalance. This is because the node voltage is influenced by many factors such as the node current, source voltage, and the loads connected to other nodes. For example, if the source voltage is severely unbalanced due to the unbalanced loads connected to other nodes, the improvement in current unbalance of the node employing an SOP with the proposed

control strategy does not mean that the node voltage unbalance can be compensated greatly. However, the control of three-phase current unbalance compensation of the node is beneficial to the improvement of node voltage unbalance.

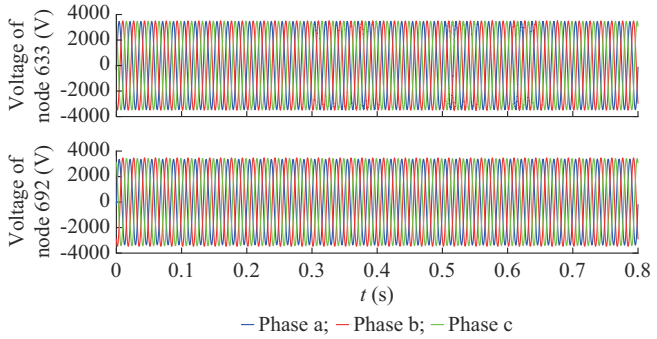

Fig. 13. Voltages of node 633 and node 692.

B. Three-phase Load Voltage Balance Control During Load Supply Restoration

The breaker in Fig. 5 is set open due to a fault. VSC 2 is controlled to feed the isolated loads connected to node 692 and node 675. From $t=0.05$ s, the common method only with positive-sequence voltage control is used. This means that the balanced three-phase voltage is generated from VSC 2. The negative-sequence voltage and zero-sequence voltage are enabled from 0.3 s and 0.4 s, respectively, with the proposed control strategy to show the improvement in the load voltage balance. VSC 1 still operates in the U_{dc}-Q control mode to stabilize the DC-link voltage. Negative-sequence current and zero-sequence current are injected from 0.4 s.

The voltage of node 692 and the reference voltage of VSC 2 are shown in Fig. 14. The positive-sequence, negative-sequence, and zero-sequence components of the reference voltage of VSC 2 are shown in Fig. 15. The output current of VSC 2 is shown in Fig. 16. Due to the unbalanced loads, only positive-sequence voltage control results in unbalanced three-phase current and voltage of node 692. With the negative-sequence and zero-sequence voltage control proposed from VSC 2, the voltage unbalance of node 692 is compensated successfully from 0.4 s.

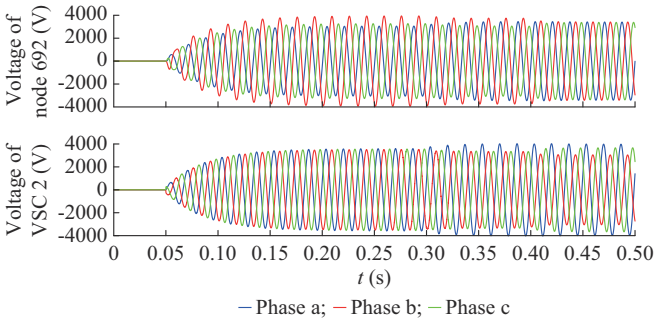

Fig. 14. Voltage of node 692 and reference voltage of VSC 2.

The DC-link voltage is shown in Fig. 17, and the output current of VSC 1 is shown in Fig. 18. Once the service restoration is achieved with VSC 2 control from 0.05 s, the active power output of VSC 2 leads to the DC-link voltage dropping. With positive-sequence current control of VSC 1, the DC-link voltage is regulated around its rated value successfully at last.

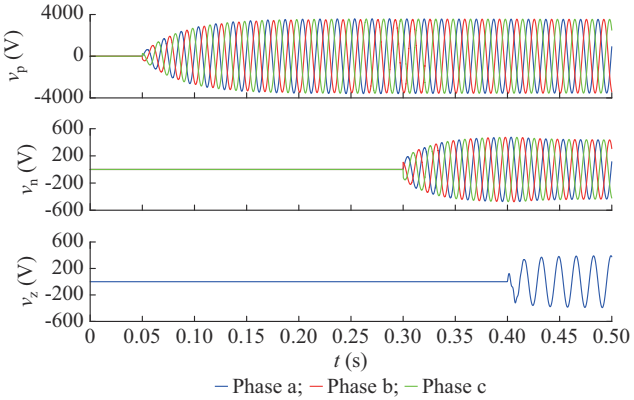

Fig. 15. Positive-sequence, negative-sequence, and zero-sequence components of reference voltage of VSC 2.

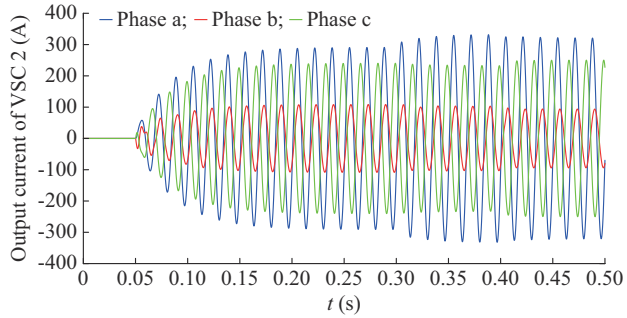

Fig. 16. Output current of VSC 2 during load supply restoration.

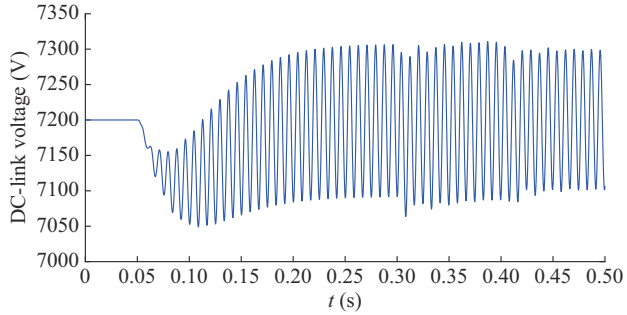

Fig. 17. DC-link voltage during load supply restoration.

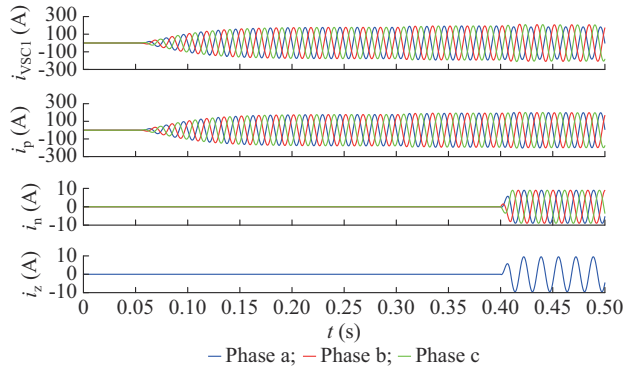

Fig. 18. Output current of VSC 1.

The current of node 633 is shown in Fig. 19. After $t=0.05$ s, the change of positive-sequence output current of VSC 1 leads to the increased current of node 633. Though VSC 2 operates in the U_{ac}-θ control mode, the current of node 633 is still controlled to be balanced successfully with the negative-sequence and zero-sequence current injection from VSC 1.

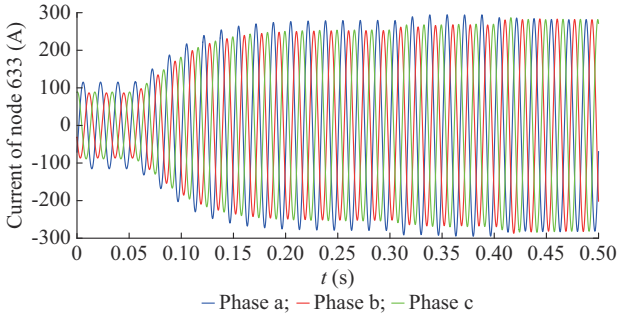

Fig. 19. Current of node 633 during load supply restoration.

V. Experimental Results

The hardware-in-the-loop experiment based on StarSim HIL is conducted to validate the voltage unbalance compensation control proposed in this paper, and the setup is shown in Fig. S1 in Supplementary Material [33]. A simplified IEEE 13-bus test feeder and an SOP with the detailed model are simulated by a real-time hardware-in-the-loop system based on NI-PXIe-1071 with the time step of 1 μs. A TMS320F28335 DSP with 10 kHz sampling frequency is used to control the SOP with the proposed control strategy. The current ratio and voltage ratio between actual signal and measured signal are 100:1 and 1000:1, respectively. Under the normal network operation condition, the negative-sequence current and zero-sequence current are generated at the same time. They are controlled to increase gradually within 0.1 s. After the node current is balanced, the power flow control is implemented to regulate the node current gradually within 0.2 s. The current of node 633 and the output current of VSC 1 are shown in Fig. S2 in Supplementary Material. The current of node 692 and the output current of VSC 2 are shown in Fig. S3 in Supplementary Material. Although high-frequency harmonics are observed in the VSC output current and node current, the node unbalanced currents at both sides of SOP are compensated successfully with the proposed control strategy. With the power flow control, the balanced node currents with the same amplitude are achieved. This means that the SOP is controlled to balance the loading of the feeder effectively.

During the restoration of power supply, only the positive-sequence voltage is generated gradually from VSC 2 firstly. Then, the negative-sequence voltage control and zero-sequence voltage control are both implemented at the same time. At last, VSC 1 is controlled to compensate the unbalanced feeder current. The voltage of node 692 and the output current of VSC 2 are shown in Fig. S4 in Supplementary Material. Unbalanced three-phase loads lead to unbalanced three-phase isolated load current and voltage. Balanced three-phase isolated load voltage is obtained successfully with the proposed control strategy. The current of node 633 and the output current of VSC 1 are shown in Fig. S5 in Supplementary Material. Though VSC 2 operates in the U_{ac}-θ control mode, the feeder unbalanced three-phase current is still compensated successfully from VSC 1 finally.

Overall, from the simulation and experimental results above, the proposed control strategy has been validated. Under normal network operation conditions, the two VSCs have compensated the three-phase current unbalance of the connected nodes, contributing to the three-phase voltage unbalance mitigation of the feeder. Once the service restoration is enabled, the connected VSC has fed the unfaulted loads and regulated the load voltage to be balanced. Furthermore, the other VSC has finished the three-phase current unbalance compensation of the connected feeder successfully. Therefore, as long as a VSC operates in the P-Q or U_{dc}-Q control mode, the three-phase current unbalance of the connected feeder can be compensated with the proposed control strategy.

VI. Conclusion

In this paper, a control strategy of voltage unbalance compensation of SOPs in distribution feeders is proposed. When the distribution network is normal, the SOP has compensated the three-phase current unbalance of the connected feeder with the injection of negative-sequence current. If the distribution network is designed with the three-phase four-wire structure, zero-sequence current should also be generated. Under this condition, the generation route of zero-sequence current must be provided in terms of the circuit topology. The current can be injected from one VSC or both ones. Therefore, the compensation is independent, and the flexibility can be guaranteed. This contributes to the mitigation of three-phase voltage unbalance. It is also more convenient to achieve load balancing, based on the three-phase current of balanced feeder. In the service restoration mode, the three-phase voltage of isolated loads has been controlled to be balanced with the negative-sequence and zero-sequence voltage control, even though the loads are unbalanced. The voltage quality and network stability are expected to be improved with the proposed control strategy. Only one SOP with the proposed control strategy is studied in the IEEE 13-bus test feeder in this paper. Whether new issues will be introduced in more complex test feeders including more SOPs will be the future research topic.

References

[1] T. P. Teixeira and C. L. T. Borges, "Operation strategies for coordinating battery energy storage with wind power generation and their effects on system reliability," *Journal of Modern Power Systems and Clean Energy*, vol. 9, no. 1, pp. 190-198, Jan. 2021.

[2] M. Dehghani, M. Taghipour, G. B. Gharehpetian *et al*., "Optimized fuzzy controller for MPPT of grid-connected PV systems in rapidly changing atmospheric conditions," *Journal of Modern Power Systems and Clean Energy*, vol. 9, no. 2, pp. 376-383, Mar. 2021.

[3] A. Ali, M. U. Keerio, and J. A. Laghari, "Optimal site and size of distributed generation allocation in radial distribution network using multi-objective optimization," *Journal of Modern Power Systems and Clean Energy*, vol. 9, no. 2, pp. 404-415, Sept. 2020.

[4] F. Attanasio, S. Wasterlain, T. Pidancier *et al*., "Low voltage soft open point with energy storage: system simulation and prototype prelimi-

nary test results," in *Proceedings of International Symposium on Power Electronics, Electrical Drives, Automation and Motion*, Amalfi, Italy, Aug. 2018, pp. 254-261.
[5] N. Mahmud and A. Zahedi, "Review of control strategies for voltage regulation of the smart distribution network with high penetration of renewable distributed generation," *Renewable and Sustainable Energy Reviews*, vol. 64, pp. 582-595, Oct. 2016.
[6] S. Bruno, S. Lamonaca, G. Rotondo *et al*., "Unbalanced three-phase optimal power flow for smart grids," *IEEE Transactions on Industrial Electronics*, vol. 58, no. 10, pp. 4504-4513, Oct. 2011.
[7] A. V. Jouanne and B. Banerjee, "Assessment of voltage unbalance," *IEEE Transactions on Power Delivery*, vol. 16, no. 4, pp. 782-790, Oct. 2001.
[8] N. Daratha, B. Das, and J. Sharma, "Coordination between OLTC and SVC for voltage regulation in unbalanced distribution system distributed generation," *IEEE Transactions on Power Systems*, vol. 29, no. 1, pp. 289-299, Jan. 2014.
[9] H. Ji, C. Wang, P. Li *et al*., "Robust operation of soft open points in active distribution networks with high penetration of photovoltaic integration," *IEEE Transactions on Sustainable Energy*, vol. 10, no. 1, pp. 280-289, Jan. 2019.
[10] T. Lee, S. Hu, and Y. Chan, "D-STATCOM with positive-sequence admittance and negative-sequence conductance to mitigate voltage fluctuations in high-level penetration of distributed-generation systems," *IEEE Transactions on Industrial Electronics*, vol. 60, no. 4, pp. 1417-1428, Apr. 2013.
[11] S. Deshmukh, B. Natarajan, and A. Pahwa, "Voltage/Var control in distribution networks via reactive power injection through distributed generators," *IEEE Transactions on Smart Grid*, vol. 3, no. 3, pp. 1226-1234, Sept. 2012.
[12] M. B. Shafik, H. Chen, G. I. Rashed *et al*., "Adequate topology for efficient energy resources utilization of active distribution networks equipped with soft open points," *IEEE Access*, vol. 7, pp. 99003-99016, Jul. 2019.
[13] H. Ji, C. Wang, P. Li *et al*., "An enhanced SOCP-based method for feeder load balancing using the multi-terminal soft open point in active distribution networks," *Applied Energy*, vol. 208, pp. 986-995, Dec. 2017.
[14] J. M. Bloemink and T. C. Green, "Increasing distributed generation penetration using soft normally-open points," in *Proceedings of IEEE PES General Meeting*, Minneapolis, USA, Sept. 2010, pp. 1-8.
[15] N. Bottrell, P. Lang, and T. Green, "Algorithm for soft open points to solve thermal and voltage constraints in low-voltage distribution networks," *CIRED-Open Access Proceedings Journal*, vol. 2017, no. 1, pp. 1567-1570, Oct. 2017.
[16] P. Li, H. Ji, C. Wang *et al*., "Coordinated control method of voltage and reactive power for active distribution networks based on soft open point," *IEEE Transactions on Sustainable Energy*, vol. 8, no. 4, pp. 1430-1442, Oct. 2017.
[17] W. Cao, J. Wu, and N. Jenkins, "Feeder load balancing in MV distribution networks using soft normally-open points," in *Proceedings of 5th IEEE PES Innovative Smart Grid Technologies Europe*, Istanbul, Turkey, Feb. 2015, pp. 1-6.
[18] L. Lin, J. He, and C. Xu, "Analysis on circulating current and split capacitor voltage balance for modular multilevel converter based three-phase four-wire split capacitor DSTATCOM," *Journal of Modern Power Systems and Clean Energy*, vol. 9, no. 3, pp. 657-667, May 2021.
[19] M. Ismail, E. Hassane, E. M. Hassan *et al*., "Power losses minimization in distribution system using soft open point," in *Proceedings of 1st International Conference on Innovative Research in Applied Science, Engineering and Technology*, Meknes, Morocco, Apr. 2020, pp. 1-8.
[20] H. Hafezi and H. Laaksonen, "Autonomous soft open point control for active distribution network voltage level management," in *Proceedings of IEEE Milan PowerTech*, Milan, Italy, Aug. 2019, pp. 1-6.
[21] H. Yang, Y. Cai, Z. Qu *et al*., "Key techniques and development trend of soft open point for distribution network," *Automation of Electric Power Systems*, vol. 42, no. 7, pp. 153-165, Apr. 2018.
[22] M. B. Shafik, G. I. Rashed, and H. Chen, "Optimizing energy savings and operation of active distribution networks utilizing hybrid energy resources and soft open points: case study in Sohag, Egypt," *IEEE Access*, vol. 8, pp. 28704-28717, Jan. 2020.
[23] S. Ouyang, J. Liu, Y. Yang *et al*., "DC voltage control strategy of three-terminal medium-voltage power electronic transformer-based soft normally open points," *IEEE Transactions on Industrial Electronics*, vol. 67, no. 5, pp. 3684-3695, May 2020.
[24] P. Li, H. Ji, C. Wang *et al*., "Optimal operation of soft open points in active distribution networks under three-phase unbalanced conditions," *IEEE Transactions on Smart Grid*, vol. 10, no. 1, pp. 380-391, Jan. 2019.
[25] H. Xiao, W. Pei, and L. Kong, "Optimal sizing and siting of soft open point for improving the three phase unbalance of the distribution network," in *Proceedings of IEEE 21st International Conference on Electrical Machines and Systems*, Jeju, Korea, Nov. 2018, pp. 1-6.
[26] W. Cao, J. Wu, N. Jenkins *et al*., "Benefits analysis of soft open points for electrical distribution network operation," *Applied Energy*, vol. 165, pp. 36-47, Mar. 2016.
[27] J. M. Bloemink and T. C. Green, "Increasing photovoltaic penetration with local energy storage and soft normally-open points," in *Proceedings of IEEE PES General Meeting*, Detroit, USA, Oct. 2011, pp. 1-8.
[28] M. B. Shafik, G. I. Rashed, H. Chen *et al*., "Reconfiguration strategy for active distribution networks with soft open points," in *Proceedings of 14th IEEE Conference on Industrial Electronics and Applications*, Xi'an, China, Sept. 2019, pp. 330-334.
[29] P. Cong, W. Tang, C. Lou *et al*., "Multi-stage coordination optimisation control in hybrid AC/DC distribution network with high-penetration renewables based on SOP and VSC," *The Journal of Engineering*, vol. 2019, no. 16, pp. 2725-2731, Mar. 2019.
[30] R. You, X. Yuan, X. Li *et al*., "A multi-rotor medium-voltage wind turbine system and its control strategy," *Renewable Energy*, vol. 186, pp. 366-377, Mar. 2022.
[31] E. Robles, S. Ceballos, J. Pou *et al*., "Variable-frequency grid-sequence detector based on a quasi-ideal low-pass filter stage and a phase-locked loop," *IEEE Transactions on Power Electronics*, vol. 25, no. 10, pp. 2552-2563, Oct. 2010.
[32] M. Hojo, Y. Iwase, T. Funabashi *et al*., "A method of three-phase balancing in microgrid by photovoltaic generation systems," in *Proceedings of 13th International Power Electronics and Motion Control Conference*, Poznan, Poland, Sept. 2008, pp. 2487-2491.
[33] Q. Zhang, Y. Zeng, Y. Liu *et al*., "An improved distributed cooperative control strategy for multiple energy storages parallel in islanded DC microgrid," *IEEE Journal of Emerging and Selected Topics in Power Electronics*, vol. 10, no. 1, pp. 455-468, Feb. 2022.

Rui You received the B.S. degree in electrical engineering from Qingdao University, Qingdao, China, in 2006, the M.S. degree in electrical engineering from Shanghai Jiao Tong University, Shanghai, China, in 2009, and the Ph.D. degree in electrical engineering from Tsinghua University, Beijing, China, in 2015. From October 2012 to November 2013, he was a Guest Ph.D. student with the Department of Wind Energy, Technical University of Denmark, Roskilde, Denmark. He joined Qingdao University, Qingdao, China, in 2015 as an Assistant Professor, where he is currently an Associate Professor. His research interests include wind turbine control, photovoltaic system control, distributed generation, and microgrid.

Xiaonan Lu received the B.E. and Ph.D. degrees in electrical engineering from Tsinghua University, Beijing, China, in 2008 and 2013, respectively. From September 2010 to August 2011, he was a Guest Ph.D. student with the Department of Energy Technology, Aalborg University, Aalborg, Denmark. From October 2013 to December 2014, he was a Postdoctoral Research Associate with the Department of Electrical Engineering and Computer Science, University of Tennessee, Knoxville, USA. From January 2015 to July 2018, he was with Argonne National Laboratory, first as a Postdoctoral Appointee and then as an Energy Systems Scientist. In July 2018, he joined the College of Engineering, Temple University, Philadelphia, USA, as an Assistant Professor. He is also the recipient of the 2020 Young Engineer of the Year Award in the IEEE Philadelphia Section. He serves as the Vice Chair of the Industrial Power Converters Committee in the IEEE Industry Applications Society. His research interests include modeling and control of power electronic inverters, hybrid AC and DC microgrids, and real-time hardware in-the-loop simulation.